Received: 10 July 2022 | Revised: 29 September 2022 | Accepted: 2 October 2022

DOI: 10.1111/jace.18839

Journal of the American Ceramic Society

RESEARCH ARTICLE

Thermally enhanced dislocation density improves both hardness and fracture toughness in single-crystal $SrTiO_3$

Mostafa Negm Salem | **Kuan Ding** | **Jürgen Rödel** | **Xufei Fang**

Department of Materials and Earth Sciences, Technical University of Darmstadt, Darmstadt, Germany

Correspondence
Xufei Fang, Department of Materials and Earth Sciences, Technical University of Darmstadt, Alarich-Weiss-Str. 2, 64287 Darmstadt, Germany.
Email: fang@ceramics.tu-darmstadt.de

Funding information
DFG, Grant/Award Numbers: 414179371, 418649505; Athene Young Investigator Programme

Abstract

Dislocation-tuned functionality in ceramic oxides for potential versatile applications gains increasing attention. As the widespread chemical doping suffers from poor temperature stability, dislocations in well-controlled mesoscopic structure may be an alternative to thermally stable intrinsic doping features. To this end, the dislocation density in plastic zones introduced by cyclic Brinell indentation is considered under thermal annealing conditions. The considerably enhanced dislocation density due to thermal treatment is found to impact both microhardness and fracture toughness, albeit only to a modest degree. The mechanistic understanding centers around enhanced mobility and multiplication of the pre-engineered dislocations at elevated temperatures driven by the residual indentation stress, as well as the strengthened interaction of point defects and dislocations at high temperature.

KEYWORDS
dislocation, fracture toughness, hardness, strontium titanate, thermal treatment

1 | INTRODUCTION

In light of the increasing research interest in dislocation-tuned functional properties such as electrical conductivity,[1] superconductivity,[2] thermal conductivity,[3] and ferroelectric properties[4] in oxides, two pertinent questions arise: (1) Are the obtained dislocation structures stable over temperature and time? (2) How are the mechanical properties affected by the built-in dislocation structure?

In this work, we correlate thermal stability of dislocations with attendant changes in mechanical properties. It has been argued that dislocations are thermodynamically more stable than point defects. Hence, they are at an advantage at high temperatures over common statistical chemical doping, which is the current method of choice for a multitude of applications. For example, Adepalli et al.[5] asserted that dislocations are thermally stable even at 1200°C while studying the dislocation-tuned electrical conductivity in polycrystalline $SrTiO_3$. However, no systematic studies on the dislocation structure evolution were contemplated as their focus was on the electrical conductivity.[6]

It is well known that thermal treatment at higher temperatures can drastically change the dislocation structure in metallic materials (recovery, recrystallization, and dislocation annihilation).[6] In contrast, much less is known about the thermal effect on the evolution of pre-engineered, room-temperature (RT) dislocations in ceramics. Due to strong ionic and covalent bond-

ing, most ceramics are plastically deformable only at high temperatures through uniaxial compression tests or creep tests.[7–9] In fact, high-temperature deformation has been so far one of the most commonly adopted methods to engineer dislocations in oxides and harness the functionality.[1,4,10] Under such circumstances, the combination of external mechanical loading and thermal heating during deformation makes it challenging to pinpoint the thermal effect on the dislocation structure evolution.

Recent RT plastic deformation in ceramic oxides has found surprising success in $SrTiO_3$, which consecutively has been used as a model material for dislocation-tuned functionality studies.[11–14] Single-crystal $SrTiO_3$ is plastically deformable at RT from bulk scale[15] to mesoscale[16] and down to micro-/nanoscale,[17–19] offering a variety of choices to introduce dislocations into the samples without crack formation. It is therefore straightforward to first generate dislocations in $SrTiO_3$ at RT then thermally treat the dislocation-rich samples at high temperature to investigate the dislocation structure evolution, as reported in ceramics with rock salt structure. For instance, by using a double-etching technique, Gilman and Johnston[20] pointed out that some dislocations could glide, whereas others would climb upon annealing a deformed single-crystal LiF at 400°C for 16 h. Keh[21] reported recovery of RT indented MgO crystals at temperatures above 1000°C. He observed an extension of edge dislocations along the dislocation arms into the undeformed region and non-crystallographic dispersion of screw dislocations outside the pre-induced dislocation arms. Besides dislocation glide and climb, recrystallization and subgrain boundary formation may also occur, as briefly reviewed by Kruger[22] for plastically deformed single-crystal LiF and NaCl.

Here, we study the dislocation structure evolution in $SrTiO_3$ at 1100°C. To exclude the complexity of grain boundaries and dopants, we used single-crystal undoped $SrTiO_3$ for all tests. For practical reasons, considering the high price of large-piece single-crystal $SrTiO_3$ and the difficulty of handling micro-/nanoscale indentation imprints, we adopt the mesoscale plastic deformation method most recently introduced by Okafor et al.[16] This method uses a large spherical indenter (with a diameter of 2.5 mm and a load of 1.5 kg) to indent the sample surface and generate a crack-free plastic zone (with a lateral diameter of ~200 μm and penetrating depth of ~100 μm). By adjusting the number of indentation cycles, a dislocation density from ~10^{10} to ~$10^{13}/m^2$ is made available.[16] The large plastic zone offers the opportunity to study the impact of thermal treatment on dislocation structure and mechanical properties using Vickers indentation in a simple manner.

In the following sections, we first describe the experimental details on generating dislocations in a large plastic zone into single-crystal $SrTiO_3$ before the samples were thermally treated in a furnace at 1100°C for 1 and 10 h, respectively. Then the mechanical testing with Vickers indentation is presented, with the microhardness and the fracture toughness being evaluated. The dislocation etch pit method enables us to correlate the change of the mechanical properties with dislocation density/structure change. In the end, the possible mechanisms for the thermally induced increase of dislocation density, microhardness, and fracture toughness will be considered.

2 | EXPERIMENTAL PROCEDURES

2.1 | Material

Undoped single-crystal $SrTiO_3$ plates with a dimension of about 2.5 mm × 2.5 mm × 1 mm are used (Alineason Materials Technology GmbH, Frankfurt am Main, Germany). The samples were polished on one side following the detailed procedure described in our previous work[17] to avoid surface mechanical deformation. Surfaces of (001) were chosen for mechanical deformation as they can be chemically etched. The dislocations were revealed by etching for 20 s in 15 ml 50% HNO_3 with 16 drops of 50% HF. For benchmarking purpose, the preexisting dislocation density in the as-received samples is contrasted to the dislocation density in the plastically deformed regions.

2.2 | Dislocation introduction

We mechanically introduce dislocations using a universal indenter machine (Karl Frank GmbH, Weinheim-Birkenau, Germany) equipped with a Brinell spherical indenter (tip diameter 2.5 mm).[16] This allows to generate a plastic zone with a lateral diameter of ~200 μm and penetrating depth of ~100 μm at RT with a load of 1.5 kg.[16] More importantly, crack formation is suppressed by the local hydrostatic compressive stresses underneath the indenter,[22] and the slip bands are formed by dislocation multiplication and motion. Single-cycle (1×) and multi-cycle indents (10 cycles or 10×, and 25 cycles or 25×) were applied on the sample surface with sufficient spacing between them to avoid overlap of the plastic zones. Our previous work[16] reported that the dislocation density increases by a factor of 1000 (from ~$10^{10}/m^2$ in the reference sample up to ~$10^{13}/m^2$ in the plastic zone with a minimum of 10 cycles). At least three identical indents were performed for each test condition for reproducibility. In the following sections, we refer to these plastic zones induced by the Brinell indenter as Brinell plastic zone.

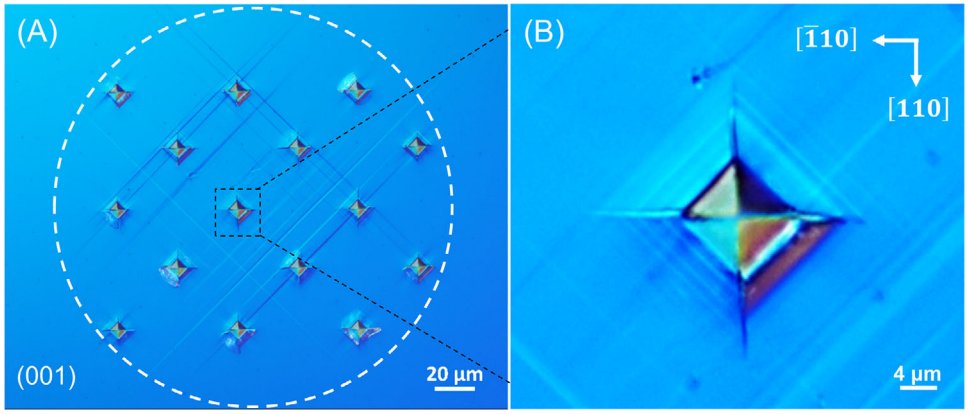

FIGURE 1 (A) Optical microscope image highlighting the checkerboard pattern of the indent array with respect to the center of the Brinell plastic zone (white dashed circle); (B) representative indent depicting the four radial cracks emerging from the corners of the Vickers indenter

2.3 | Thermal treatment

Thermal annealing was carried out in a box furnace in air (Nabertherm GmbH, Lilienthal, Germany). For uniform heat distribution in the sample, the indented samples with Brinell plastic zones were placed inside a ceramic crucible in the furnace. The temperature of $0.58T_m$ (1100°C or 1373 K, with T_m = 2353 K[23]) was chosen to have an accelerated atomic diffusion in order to observe a possible change of the dislocation structure in the samples. Holding times of 1 and 10 h and a heating rate of 10 K/min were maintained, and later the furnace was cooled.

2.4 | Mechanical testing

Microhardness was quantified using a Vickers indenter (Zwick/Roell ZHμ, Ulm, Germany). Indents were placed inside the Brinell plastic zones for both annealed and RT reference samples. At each plastic zone induced by Brinell indentation, a 3 × 5 checkerboard patterned array using a load of 25 g and 10 s dwell time was applied. A spacing of at least 40 μm in both the x and y direction minimized any mutual interference from the neighboring deformation zone (Figure 1A). The Vickers indents have been aligned so that the diagonals of each indent coincide with [1 1 0] and [$\bar{1}$ 1 0] directions (Figure 1B). The effect of the spatial distance of each Vickers indent with respect to the center of the Brinell plastic zone is neglected due to the fact that the dislocation density inside the Brinell plastic zone is constant.[16] Moreover, for statistical analysis, we recorded the crack length in both [1 1 0] and [$\bar{1}$ 1 0] directions (Figure 1B) for more than 20 indents in each test condition.

2.5 | Surface morphology and characterization

Slip traces inside the Brinell plastic zones and their evolution succeeding the thermal treatment for each cycle number (1×, 10×, and 25×) were observed by an optical microscope (ZEISS Axio, Carl Zeiss Microscopy GmbH, Jenna, Germany). We adopted the circular differential interference contract (C-DIC) imaging mode for a better detection of surface features. After chemical etching, the etch pit analysis was carried out based on the SEM (scanning electron microscope, TESCAN MIRA3, Brno, Czech Republic) images to estimate the dislocation density. To avoid surface charging, sample surfaces were coated with a carbon layer (tens of nm in thickness) with a sputtering machine (K950X Turbo Evaporator, EMITech, Ashford, UK). Additionally, laser microscope (LEXT OLS4100, Olympus, Japan) was also used for characterizing the surface etch pits over a much larger area (hundreds of μm in width).

3 | RESULTS AND ANALYSES

3.1 | Surface morphology

We first confirm the preexisting (grown-in) dislocation density before the mechanical testing and thermal treatment. The dislocation etch pits in Figure 2 yield a preexisting dislocation density ~$10^{10}/m^2$, consistent with prior values reported for single-crystal $SrTiO_3$.[24,25]

The plastic deformation on the surfaces of the indented samples is reflected in the slip traces on the (001) surfaces

in Figure 3. All slip lines are aligned horizontally or vertically in the [100] and [010] directions, without surface cracks.[16] As $SrTiO_3$ has a cubic structure and the slip system activated at RT is {110} ⟨110⟩, it is thus confirmed that these slip traces correspond to the screw components (with the Burgers vector pointing out-of-plane) of the dislocations, which are aligned on the 45°-inclined {110} glide planes with respect to the (001) surface. These results are consistent with the 3D reconstruction of the spatial dislocation arrangement reported by Javaid et al.[26] An increase in the number of indentation cycles leads to an enhanced density of slip lines, in agreement with the results by Okafor et al.[16]

We note that the C-DIC imaging mode significantly enhances the surface features such as slip traces for better recognition of the surface deformation (Figure 3). In fact, the maximum height difference even after 25 cycles at RT and after 10 h thermal treatment at 1373 K is merely 0.48 and 0.53 μm, respectively. The surface height change is demonstrated by the laser microscopy observation (Figure 4). The very small height difference across the large plastic zone (~200 μm) gives confidence that the follow-up Vickers indentation tests shall not be influenced by the curvature of the Brinell plastic zone.

3.2 | Dislocation density

Dislocation density in the plastic zone for various conditions is closely examined via etch pit method, feasible for statistical quantification. For RT indentation, the dislocation density (etch pit counts in Figure 5) increases as the cycle number increases from 1 to 25. The annealing treatment (e.g., Figure 5B1–3 for 1 h annealing) increases the dislocation density for the same number of indentation cycles. A longer annealing time (up to 10 h, Figure 5C1–3) causes an enhancement in the dislocation density.

An overview of the dislocation density is compiled in Figure 6, which quantitatively confirms that the dislocation density increases as a function of cyclic number and thermal treatment: (1) Compared to the reference density (~$10^{10}/m^2$, Figure 1), at least a 100-fold increase in the dislocation density after 1× is achieved (irrespective of the thermal treatment); (2) for the same number of indentation cycles, the density after 10 h annealing is 5–7 times higher than that induced at RT without thermal treatment; (3) a most distinct change is found between 1× indent at RT (~$2 \times 10^{12}/m^2$) and 25× indents with 10 h thermal treatment (~$7 \times 10^{13}/m^2$), giving an almost 35-fold increase; (4) when compared the reference sample and the 25× indents with 10 h thermal treatment, an increase about 7000-fold in the dislocation density is achieved. This case of highest achieved dislocation density corresponds to an average dislocation spacing of about 120 nm.

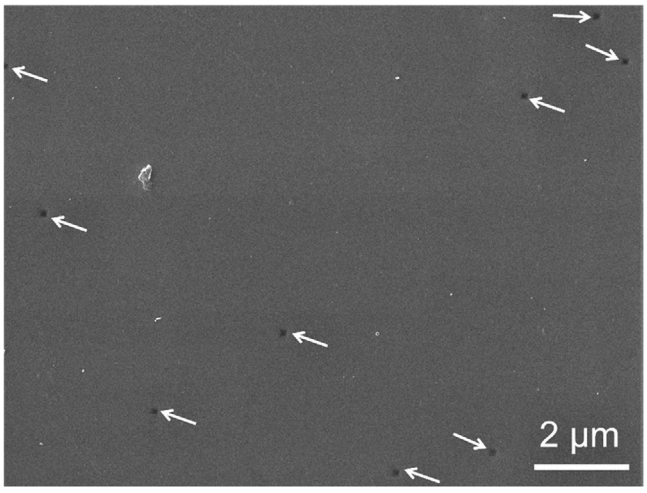

FIGURE 2 Scanning electron microscope (SEM) image depicting the dislocation etch pits (indicated by the white arrows) on the reference sample surface before mechanical testing

3.3 | Microhardness

The change of dislocation density directly impacts mechanical properties. Here, we evaluate the microhardness as a function of indentation cycle number and thermal treatment. The average values as well as the statistical distribution of the hardness are summarized in Figure 7. First, the hardness increases modestly as the number of cycles increases (under the same thermal treatment condition). For RT (black squares in Figure 7A), an increase of ~12% in the Vickers hardness is observed. Second, the hardness increases after thermal annealing for the same indentation cycle number. For instance, for 1× indents, the Vickers hardness after 10 h annealing is ~13% higher than that without annealing. In general, a longer annealing time (10 h) gives higher hardness values in comparison to the shorter annealing time (1 h). The most significant increase in hardness (~20%) falls between the 1× indent at RT and 25× indent with 10 h thermal treatment. These observations on the hardness increase are consistent with the increase in dislocation density (Figure 6).

3.4 | Indentation crack length and fracture toughness

A quantification of indentation crack lengths in the Vickers indentation tests provides a clear trend (Figure 8): The crack length decreases as the dislocation density increases.

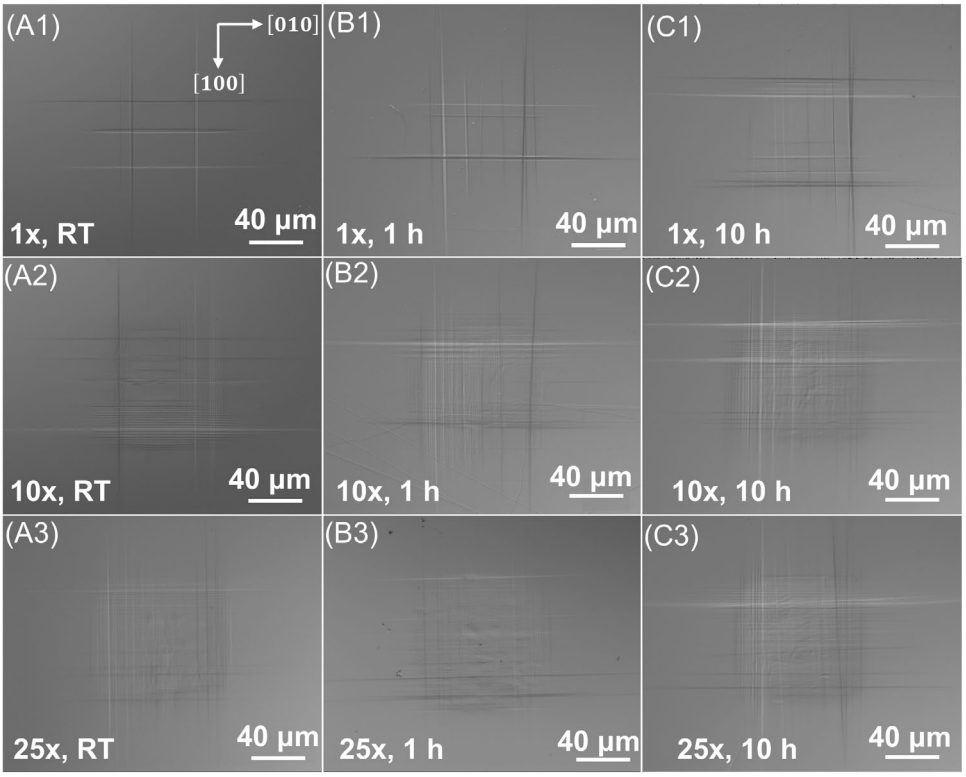

FIGURE 3 Surface slip trace patterns for the indented regions: (A1–3) room temperature (RT) without annealing; (B1–3) thermal treatment at 1373 K for 1 h; (C1–3) thermal treatment at 1373 K for 10 h. The horizontal and vertical slip traces are parallel to the [010] and [100] directions. Note:1×, 10×, and 25× stand for 1, 10, and 25 cycles, respectively

By comparing the crack lengths at RT (round dots in Figure 8A,B), it is noticed that there is only marginal crack shortening from 1× cycle indents to 10× cycle Brinell indents. A more obvious shortening can only be observed between the 1× cycle and 25× cycle Brinell indents. A similar trend is also found for the indents in samples thermally treated for 1 h with 1×, 10×, and 25× cycle. Most significantly, ~40% decrease of crack length (average value) is observed between RT-1× and 1 h-25× indents, with the dislocation density increased by ~10-fold between these two cases (Figure 6).

Note that the cracks for the 10-h annealed samples, particularly for the 10× and 25×, are no longer symmetrical 4-crack patterns (as in Figure 2B). In such cases, some of the Vickers indenter imprints exhibit only two or three instead of four cracks at the four corners of the indent imprint. This is likely caused by the much higher dislocation density after 10-h annealing, which may have greatly increased the damage tolerance as more dislocations are able to carry a higher degree of plastic deformation. Hence, these data are not included in Figure 8 for comparison.

We further adopt the indentation crack length method to evaluate the fracture toughness, K_{IC}. Both the half-penny crack in the Evans–Charles model[27] and the median/radial crack Lawn–Evans–Marshall model[28] for indentation cracks do not fit the crack geometry induced in $SrTiO_3$. Instead, successive polishing and etching the indented area[29] indicates that the cracks in $SrTiO_3$ are Palmqvist cracks. This is likely due to the large plasticity mediated by dislocations underneath the indent. These dislocations could have suppressed the median crack formation, reminiscent of indentation cracks in the plastically deformed regions, as was well documented in WC–Co material.[30]

For Palmqvist cracks, we adopt here Equation (1) proposed by Niihara.[31,32] This model is in principle a modification of the Evans–Charles model. Niihara et al. proposed such modification for small l/a ratio ($0.25 < l/a < 2.5$)[32]:

$$K_{IC} = 0.035 \left(\frac{l}{a}\right)^{-0.5} \left(\frac{E\phi}{H}\right)^{0.4} \left(\frac{Ha^{0.5}}{\phi}\right) \quad (1)$$

where E is the elastic modulus (264 GPa for single-crystal $SrTiO_3$ at RT [33]), l is the crack length (from the tip of the indentation imprint to the tip of the crack), a is the half-diagonal of the indentation, the constant $\phi = 3$ is adopted,[31,32] H is the hardness (converted to GPa, from the microhardness values presented in Figure 7A). In the current experiment, the calculated l/a value ranges from 0.93 to 1.4, fulfilling the requirement of $0.25 < l/a < 2.5$.

Figure 9 asserts a clear dislocation–toughening effect for cracks aligned in the [1 1 0] and [$\bar{1}$ 1 0] directions. Due to

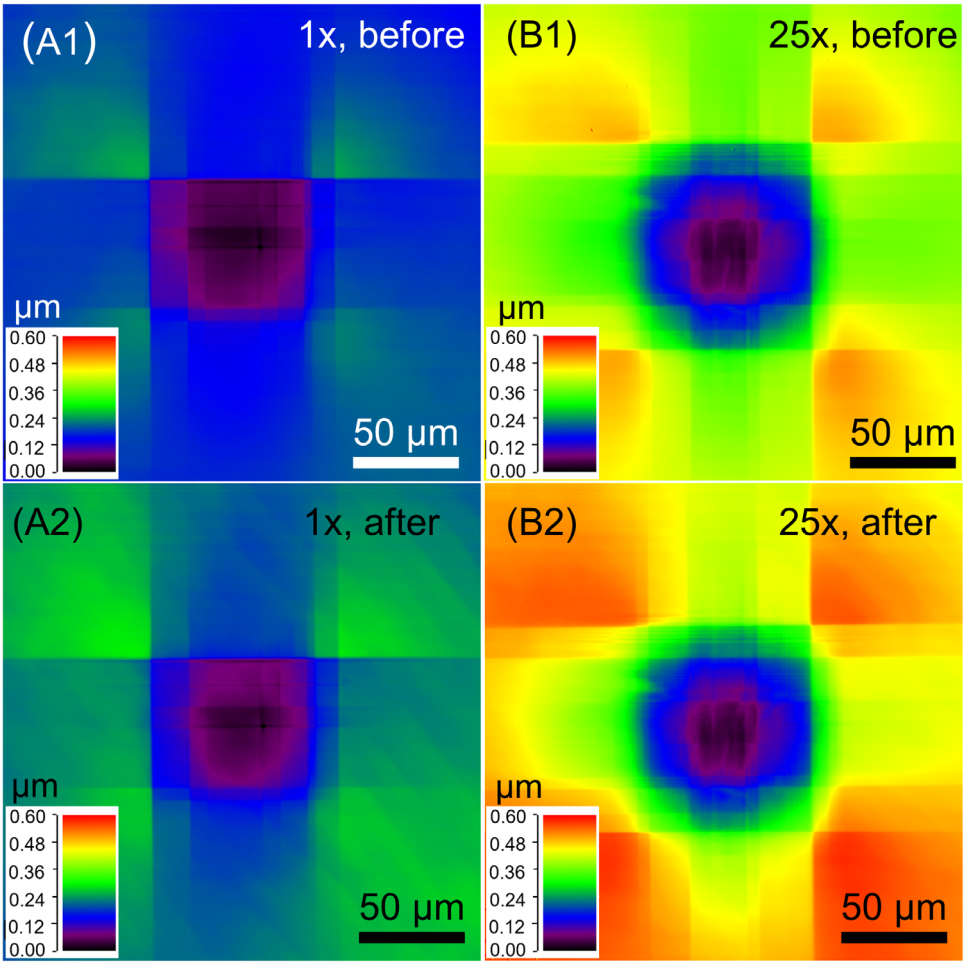

FIGURE 4 Laser microscope images for the surface topography of the plastic zones induced by a load of 1.5 kg: 1× and 25× indent before (A1 and B1) and after (A2 and B2) thermal treatment at 1373 K for 10 h. The maximum height difference for 1× and 25× indents are about 0.25 and 0.48 μm before annealing, and 0.27 and 0.53 μm after annealing at 1373 K for 10 h.

the cubic symmetry, the toughness values in the [1 1 0] and [$\bar{1}$ 1 0] directions are identical. The most dramatic change in K_{IC} was observed in Brinell plastic zones induced by 1× cycle at RT (1×-RT) and 25× cycle with 1-h annealing (25×-1 h), with an increase from 0.93 to 1.14 MPa $m^{1/2}$. Correspondingly, the dislocation density increase for these two test conditions is also the largest ($\sim 2 \times 10^{12}/m^2$ for 1×-RT and $\sim 2 \times 10^{13}/m^2$ for 25×-1 h) under these test conditions.

By combining Figures 6–9, we identify a clear trend that both microhardness and fracture toughness have been improved due to the increase of dislocation density in combination with the thermal treatment.

4 | DISCUSSION

4.1 | Thermally triggered increase of dislocation density

Interestingly, the dislocation density increased due to the thermal treatment. The underlying mechanisms are discussed as following. First of all, an increase in temperature could provide a decrease in the yield stress in $SrTiO_3$. For instance, for single-crystal $SrTiO_3$ compressed along the [001] direction, the yield stress was reported to decrease from ~125 MPa at RT to ~50 MPa at 450°C according to Patterson et al.[33] Later, Javaid et al.[34] quantified the lattice friction stress (resistance to dislocation glide) via the etch pit method, giving a value of 89 MPa for RT and 46 MPa at 350°C. These results support the notion of a decreasing resistance for dislocation glide with increasing temperature. Furthermore, according to abundant indentation studies in literature,[35] the plastic zone underneath the Brinell indent possesses a residual stress state, which can undergo relaxation due to dislocation motion or atomic diffusion during thermal treatment. It is therefore hypothesized that the pre-induced dislocations in the Brinell plastic zone induced at RT continued to glide and multiply when they were thermally treated up to 1100°C, resulting in an increase in dislocation density (Figures 5–6).

To better illustrate dislocation rearrangement due to thermal treatment, we performed additional tests using

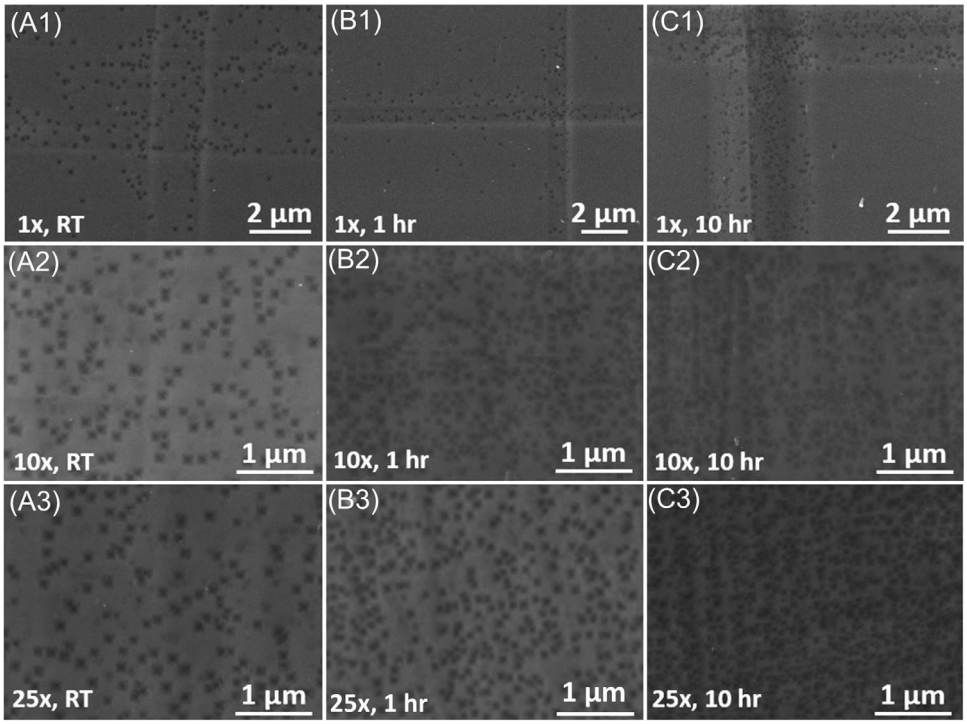

FIGURE 5 Etch-pit analyses of the dislocations introduced by Brinell indentation with different loading cycles and different thermal treatments: (A1–3) room temperature (RT) without annealing; (B1–3) thermal treatment at 1373 K for 1 h; (C1–3) thermal treatment at 1373 K for 10 h

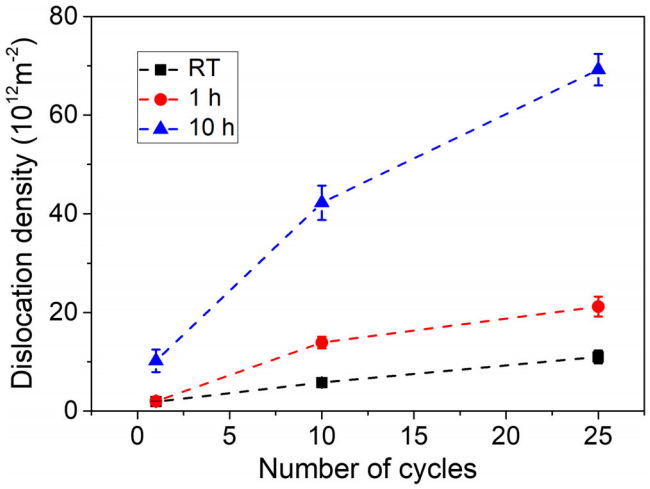

FIGURE 6 Averaged dislocation density as function of indentation cycle number and thermal treatment. The dislocation density of a reference undeformed sample is ~$10^{10}/m^2$ (in Figure 1).

Vickers indentation to induce plastic deformation and compare the dislocation structure at RT (Figure 10A) and after annealing for 1 h at 1100°C (Figure 10B). Regardless of the crack generation, using Vickers indent delivers certain advantages over large Brinell indents. Specifically, the Vickers indentation imprints serve as surface markers rendering the dislocation patterns more traceable (Figure 10A), and the edge dislocation arms (the 45° dislocation arms in the ⟨110⟩ directions) can also be induced due to the higher stress under the Vickers indent. For best comparison, we adopt the double-etching technique to track the dislocation structure around the same Vickers indent. The comparison between Figure 10A,B clearly highlights numerous new dislocation etch pits emerged outside of the original dislocation zone. Besides the increased dislocation density after thermal treatment, we also observed another two interesting features: (1) Numerous horizontal and vertical straight lines appeared among the rosette arms that mainly consist of edge dislocation components (yellow rectangles in Figure 10A,B),[24,26] yet the thermal treatment did not induce any further gliding of such dislocations in the ⟨1 1 0⟩ direction. The end positions of the edge dislocation component were marked with red circles in Figure 10A,B. This strongly suggests dislocations climb out of the RT slip planes after thermal treatment; (2) curly, bent etch pit and line patterns originate from the regions where mainly screw dislocation components previously resided (green rectangles in Figure 10A,B),[24,26] and the positions for the tips of such dislocation arms (red arrows in Figure 10A,B) extended and moved by about 50 μm due to thermal treatment. This change of the configuration for the screw-type dislocations is consistent with the report by Keh,[21] who observed a non-crystallographic dispersion of screw dislocations outside the pre-induced

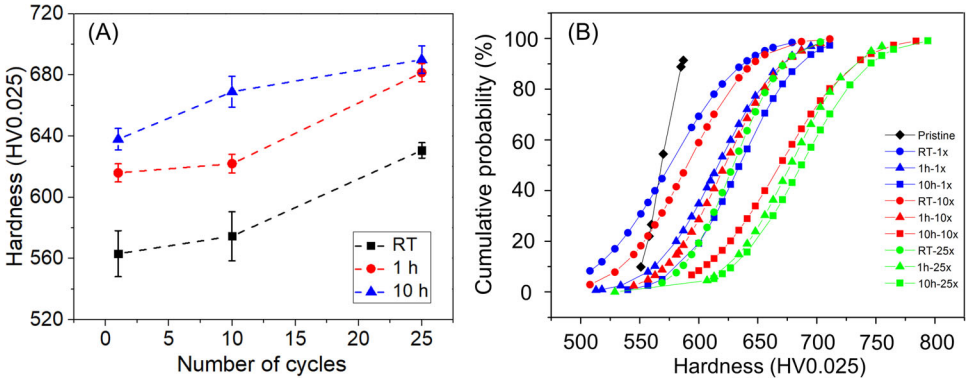

FIGURE 7 (A) averaged Vickers microhardness versus. Brinell indentation cycles; (B) cumulative probability plot of all hardness data for various indentation cycle numbers and temperatures

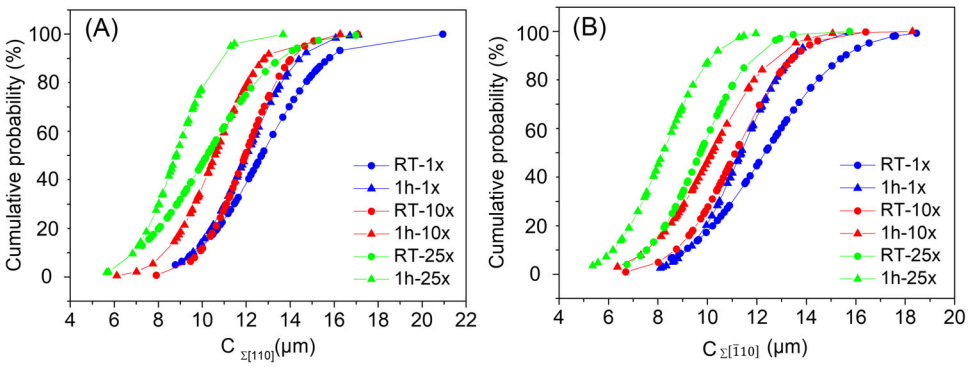

FIGURE 8 Cumulative probability plots of crack length in (A) $C_{\sum[110]}$ and (B) $C_{\sum[-110]}$ directions. Note the sign $\sum$ indicates the sum of two cracks in each direction for each indent.

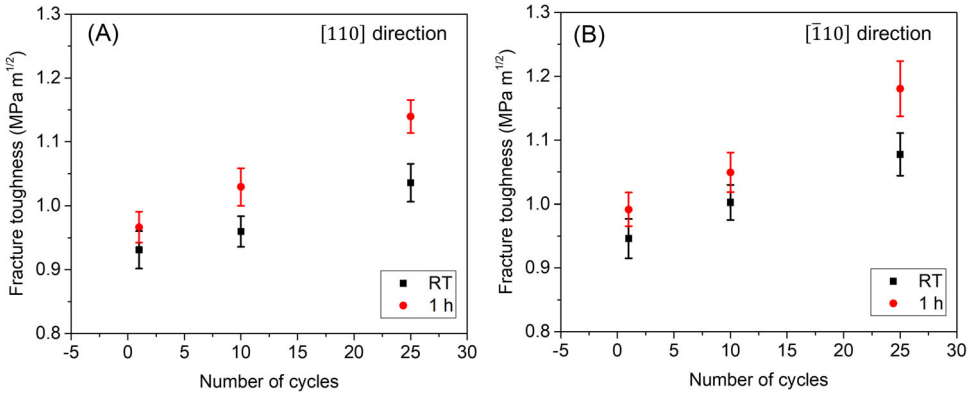

FIGURE 9 K_{IC} as function of Brinell indentation cycles in (A) [$^{-}$110] directions and (B) [110] directions. The symbols visualize the contrast between room temperature (RT) and annealing times of 1 h. Note that the cracks for the 10-h annealed samples, particularly for the 10× and 25×, are no longer symmetrical 4-crack patterns and are hence excluded for comparison.

dislocation arms during the recovery of RT indented MgO crystals at temperatures above 1000°C. Note that the image force may tend to attract the dislocations to the free surface. A much more detailed investigation of the dislocation substructures in the future with TEM (transmission electron microscopy) analysis will shed light on the dislocation structure evolution.

The previous observations may stand in variance to the study by Bell et al.[36] on high-temperature crept rutile TiO_2. They reported a lowering of the dislocation density

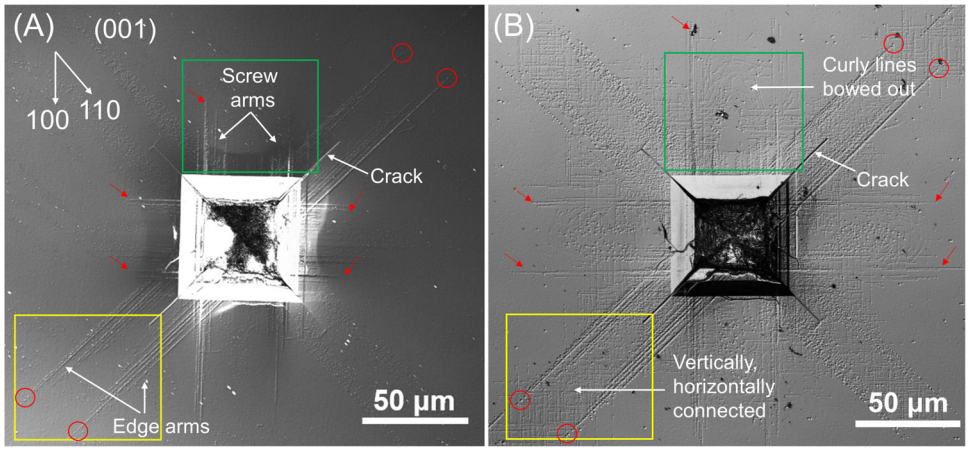

FIGURE 10 Double-etching technique to reveal dislocation structures before and after thermal treatment. (A) Dislocation etch pits around a Vickers indent imprint (500 g load) at room temperature. The dislocation etch pits align in the room-temperature {110} slip planes that intersect with the (001) surface, with the screw arms in the ⟨100⟩ directions and the edge arms in the ⟨110⟩ directions; (B) same indent as in (A) but with an additional annealing at 1373 K for 1 h, followed by a second-round chemical etching at room temperature. Abundant new dislocation etch pits appear outside the room-temperature dislocation arms.

observed as the dislocations bundled up to form subgrain boundaries or dislocation walls.[1] Considering that the conventional sintering temperature for $SrTiO_3$ is above 1673 K (1400°C), it may require a much higher temperature for the dislocations to bundle up to form subgrain boundaries or to be annealed out in $SrTiO_3$ than the present temperature (1373 K) in this work.

Similar to our results, an increase in dislocation density was reported by Johnston and Gilman in LiF,[20] and Keh[21] in indented MgO followed by thermal annealing. Worth noting is that Gilman and Johnston noted in their early dislocation study in single-crystal LiF that "fast heating or cooling rates to and from the annealing temperature introduce multitudes of additional dislocations into the crystals."[20] Yet, no definition for fast or slow heating/cooling rate was offered. The fast heating/cooling rate could potentially induce internal compressive/tensile stress to even activate the high-temperature {1 00} ⟨100⟩ slip system in $SrTiO_3$, which is possible at temperature higher than 1000 K.[37] Together with the previous issue concerning the temperatures at which the dislocations in the indented regions start to polygonise or annihilate, these remaining open questions will be undertaken in the future to extend the current study.

4.2 | Thermally triggered increase in microhardness

The microhardness is a measurement of the deformability of the material underneath the indenter. For dislocation-mediated plastic deformation, dislocation–dislocation interaction and dislocation-point defect interaction are possible mechanisms contributing to the hardness increase. The former increases the work hardening or Taylor hardening, resulting in a higher hardness through a higher dislocation density; the latter decreases the dislocation mobility by pinning the dislocations, most likely through the segregation of point defects at the dislocations, leading to a solution hardening effect or forming a Cottrell cloud (or alike) surrounding the dislocations. This is directly reflected by the hardness increase between 1×-RT and 1×-1 h, where the dislocation density is almost the same ($2 \times 10^{12}/m^2$, in Figure 6), but the hardness is increased by ~10% after 1 h annealing at 1373 K. Consider the current annealing temperature is higher than 0.5 T_m of $SrTiO_3$, the annealing process could significantly accelerate the diffusion of point defects to the dislocations and remain "locked in" upon cooling the samples.

The pinning of dislocations after thermal treatment was previously reported by Keh[21] in single-crystal MgO and Johnston and Gilman[38] in single-crystal LiF. In both cases, they argued that such effect is most likely due to impurities. The current authors have proposed that oxygen vacancies may segregate to dislocations and pin the dislocations at RT, hence, reducing the dislocation mobility as evidenced by the indentation creep tests on single-crystal $SrTiO_3$ with higher oxygen vacancy concentrations.[17,19] In the current case at 1373 K, we first consider oxygen vacancies ($V_O^{\bullet\bullet}$) as the most dominant fast diffusing species in $SrTiO_3$.[19] With a diffusion coefficient D_V (1373 K) ≈ $10^{-4.5}$ cm^2/s,[39] we estimate a diffusion length of ~3 mm for 1 h and ~10 mm for 10 h by using Fick's law $L = \sqrt{D_V(T)t}$, with L being the diffusion length, D_V the diffusion coefficient, and t the time. In both cases, the diffusion lengths are much larger than the sample thickness

(1 mm) as well as the plastic zone size. This estimation, therefore, excludes oxygen vacancies as a limiting factor for pinning the dislocations at the annealing temperature (1373 K).

At temperatures higher than 1300 K, strontium vacancies also exhibit sufficient mobility.[39] The diffusion coefficient for strontium vacancy (V''_{Sr}) in $SrTiO_3$ at the annealing temperature 1373 K is D_V (1373 K) $\approx 10^{-16}$ cm^2/s in $SrTiO_3$ with 0.2 at% Nb.[40] Assume that the 0.2 at% Nb doping does not drastically change the diffusion rate of strontium vacancy (as we use undoped $SrTiO_3$ in the present work), following Fick's law we calculate the diffusion length for strontium vacancy to be ~6 nm for 1-h and ~20 nm for 10-h annealing. Such diffusion lengths are therefore comparable to the aforementioned average spacing of dislocations, especially for the case of 10 h annealing with a dislocation spacing of about 120 nm. The diffusion of Sr vacancies to the dislocations at high temperature and then being frozen at RT after cooling may reduce the dislocation mobility and contribute to the hardness increase.

4.3 | Thermally triggered increase in fracture toughness

The combination of Figures 6 and 9 indicates a direct correlation between fracture toughness enhancement and dislocation density increase due to thermal treatment at 1373 K. Dislocation-based toughening in ceramics is rarely addressed in literature except for a few attempts.[25,41–43] In order to achieve effective dislocation toughening, spontaneous crack-tip dislocation emission and crack-tip blunting are required,[44] which is energetically not feasible in most brittle ceramics.[45] Here, for single-crystal $SrTiO_3$ that can be plastically deformed higher than 10% plastic strain at RT,[46] spontaneous crack-tip dislocation emission was not observed.[24] This discourages the true realization of appreciable intrinsic toughening using dislocations in $SrTiO_3$ at RT. However, by prior engineering of preexisting dislocations via the Brinell indentation method, we generate high-density and mobile dislocations inside the plastic zone. If cracks are induced inside such plastic zones, the pre-engineered dislocations are expected to consume energy and shield the crack tip to suppress crack propagation. However, only less than ~10% increase is achieved for dislocation-rich samples engineered at RT, regardless of the fact that the dislocation density has increased by more than three orders of magnitude.

Concurrently, the fracture toughness value has increased by ~20% after thermal treatment. The underlying reason for this increase could be (1) the residual stress generated during the generation of the large Brinell plastic zone, or (2) the dislocation density increase and the dislocation substructure change (Figure 10). The residual stress is not likely contributing to the toughening due to the fact that our annealing procedure rather would reduce residual stress. Particularly, it has been demonstrated that for the 1× Brinell indent, the fracture toughness increases after 1-h annealing at 1373 K (Figure 9) although the dislocation density is almost the same at RT (Figure 6).

Furthermore, we note that for samples thermally treated for 10 h, the crack pattern was not symmetrical anymore, but with only two or three shorter cracks from the indenter edge. This indicates an increased damage tolerance. It was recently reported that[25] provided the dislocation density is increased to ~$10^{15}/m^2$ in the sample surface via surface grinding,[47] the crack formation can even be completely suppressed during Vickers indentation (e.g., with a load of 10 g) on the (001) surfaces in $SrTiO_3$.

5 | CONCLUSIONS

A protocol has been put forward that combines cyclic Brinell indentation and high-temperature annealing in order to provide large plastic zones with dislocation densities approaching ~$10^{14}/m^2$ in single-crystal $SrTiO_3$. The large Brinell plastic zones afford experimental evaluation of both microhardness and fracture toughness using the indentation crack length technique. Although the dislocation density can be further enhanced by a factor of up to 35 with optimized thermal treatment, both microhardness and fracture toughness provide a modest, but statistically significant enhancement of at most 20%.

The changes in mechanical properties are hypothesized to be related to enhanced dislocation movement and multiplication under thermal activation likely driven by the residual stress. Specifically, the hardening is suggested to be enhanced due to the increase in dislocation density and an interaction of point defects and dislocations.

ACKNOWLEDGMENTS

The financial support by DFG (Grant Numbers: 414179371 and 418649505) is gratefully acknowledged. X. F. also acknowledges thes for financial support by the Athene Young Investigator Programme at TU Darmstadt for independent basic research. We thank Prof. K. Durst at TU Darmstadt for access to the laser microscope and SEM, O. Preuß for taking the laser microscope image, Dr. L. Porz for experimental demonstration of the Palmqvist-type crack, Prof. A. Nakamura at Osaka University, Dr. Till Frömling at TU Darmstadt, and Prof. Wenjun Lu at Southern University of Science and Technology for helpful discussions.

Open Access funding enabled and organized by Projekt DEAL.

ORCID

Xufei Fang https://orcid.org/0000-0002-3887-0111

REFERENCES

1. Muhammad QK, Porz L, Nakamura A, Matsunaga K, Rohnke M, Janek J, et al. Donor and acceptor-like self-doping by mechanically induced dislocations in bulk TiO_2. Nano Energy. 2021;85:105944.
2. Hameed S, Pelc D, Anderson ZW, Klein A, Spieker RJ, Yue L, et al. Enhanced superconductivity and ferroelectric quantum criticality in plastically deformed strontium titanate. Nat Mater. 2022;21:54–61.
3. Khafizov M, Pakarinen J, He L, Hurley DH. Impact of irradiation induced dislocation loops on thermal conductivity in ceramics. J Am Ceram Soc. 2019;102(12):7533–42.
4. Höfling M, Zhou X, Riemer LM, Bruder E, Liu B, Zhou L, et al. Control of polarization in bulk ferroelectrics by mechanical dislocation imprint. Science. 2021;372:961–4.
5. Adepalli KK, Yang J, Maier J, Tuller HL, Yildiz B. Tunable oxygen diffusion and electronic conduction in $SrTiO_3$ by dislocation-induced space charge fields. Adv Funct Mater. 2017;27(22):1700243.
6. Gottstein G. Materialwissenschaft und Werkstofftechnik. 4th ed. Heidelberg, Germany: Springer; 2014.
7. Mitchell TE, Lagerlöf KPD, Heuer AH. Dislocations in ceramics. Mater Sci Technol. 1985;1(11):944–9.
8. Pelleg J. Creep in ceramics. Heidelberg, Germany: Springer; 2017.
9. Mitchell T, Heuer A. Dislocations and mechanical properties of ceramics. Dislocations in Solids. 2004;12, 339–402.
10. Nakamura A, Matsunaga K, Tohma J, Yamamoto T, Ikuhara Y. Conducting nanowires in insulating ceramics. Nat Mater. 2003;2(7):453–6.
11. Porz L, Fromling T, Nakamura A, Li N, Maruyama R, Matsunaga K, et al. Conceptual framework for dislocation-modified conductivity in oxide ceramics deconvoluting mesoscopic structure, core, and space charge exemplified for $SrTiO_3$. ACS Nano. 2021;15:9355–67.
12. Souza RAD. Transport properties of dislocations in $SrTiO_3$ and other perovskites. Curr Opin Solid State Mater Sci. 2021;25:100923.
13. Gao P, Yang S, Ishikawa R, Li N, Feng B, Kumamoto A, et al. Atomic-scale measurement of flexoelectric polarization at $SrTiO_3$ dislocations. Phys Rev Lett. 2018;120(26):267601.
14. Szot K, Rodenbücher C, Bihlmayer G, Speier W, Ishikawa R, Shibata N, et al. Influence of dislocations in transition metal oxides on selected physical and chemical properties. Crystals. 2018;8(6):241–317.
15. Brunner D, Taeri-Baghbadrani S, Sigle W, Rühle M. Surprising results of a study on the plasticity in strontium titanate. J Am Ceram Soc. 2001;84(5):1161–3.
16. Okafor C, Ding K, Zhou X, Durst K, Rödel J, Fang X. Mechanical tailoring of dislocation densities in $SrTiO_3$ at room temperature. J Am Ceram Soc. 2022;105:2399–402.
17. Stich S, Ding K, Muhammad QK, Porz L, Minnert C, Rheinheimer W, et al. Room-temperature dislocation plasticity in $SrTiO_3$ tuned by defect chemistry. J Am Ceram Soc. 2022;105:1318–29.
18. Fang X, Bishara H, Ding K, Tsybenko H, Porz L, Höfling M, et al. Nanoindentation pop-in in oxides at room temperature: dislocation activation or crack formation? J Am Ceram Soc. 2021;104:4728–41.
19. Fang X, Ding K, Janocha S, Minnert C, Rheinheimer W, Frömling T, et al. Nanoscale to microscale reversal in room-temperature plasticity in $SrTiO_3$ by tuning defect concentration. Scr Mater. 2020;188:228–32.
20. Gilman JJ, Johnston WG. Observations of dislocation glide and climb in lithium fluoride crystals. J Appl Phys. 1956;27(9):1018–22.
21. Keh AS. Dislocations in indented magnesium oxide crystals. J Appl Phys. 1960;31(9):1538–45.
22. Kruger K. Texture development in axissymmetric forging and plane strain compression of lithium fluoride. West Lafayette, Indiana: Purdue University; 1999.
23. Ohta H. Thermoelectrics based on strontium titanate. Mater Today. 2007;10(10):44–9.
24. Fang X, Ding K, Minnert C, Nakamura A, Durst K. Dislocation-based crack initiation and propagation in single-crystal $SrTiO_3$. J Mater Sci. 2021;56:5479–92.
25. Porz L, Klomp AJ, Fang X, Li N, Yildirim C, Detlefs C, et al. Dislocation-toughened ceramics. Mater Horiz. 2021;8:1528–37.
26. Javaid F, Stukowski A, Durst K. 3D dislocation structure evolution in strontium titanate: spherical indentation experiments and MD simulations. J Am Ceram Soc. 2017;100(3):1134–45.
27. Evans AG, Charles EA. Fracture toughness determinations by indentation. J Am Ceram Soc. 1976;59(7–8):371–2.
28. Lawn BR, Evans AG, Marshall DB. Elastic/plastic indentation damage in ceramics: the median/radial crack system. J Am Ceram Soc. 1980;63:574.
29. Javaid F, Bruder E, Durst K. Indentation size effect and dislocation structure evolution in (001) oriented $SrTiO_3$ Berkovich indentations: HR-EBSD and etch-pit analysis. Acta Mater. 2017;139:1–10.
30. Shetty DK, Wright IG, Mincer PN, Clauer AH. Indentation fracture of WC-Co cermets. J Mater Sci. 1985;20:1873–82.
31. Niihara K. A fracture mechanics analysis of indentation-induced Palmqvist crack in ceramics. J Mater Sci Lett. 1983;2:221–3.
32. Niihara K, Morena R, Hasselman DPH. Evaluation of K_{Ic} of brittle solids by the indentation method with low crack-to-indent ratios. J Mater Sci Lett. 1982;1:13–6.
33. Patterson EA, Major M, Donner W, Durst K, Webber KG, Rödel J. Temperature-dependent deformation and dislocation density in $SrTiO_3$ (001) single crystals. J Am Ceram Soc. 2016;99(10):3411–20.
34. Javaid F, Johanns KE, Patterson EA, Durst K. Temperature dependence of indentation size effect, dislocation pile-ups, and lattice friction in (001) strontium titanate. J Am Ceram Soc. 2018;101(1):356–64.
35. Lawn B. Fracture of brittle solids. 2nd ed. Cambridge: Cambridge University Press; 1993.

36. Bell H, Krishnamachari V, Jones JT. Recovery of high-temperature creep-resistant substructure in rutile. J Am Ceram Soc. 1972;55:6–10
37. Taeri S, Brunner D, Sigle W, Rühle M. Deformation behaviour of strontium titanate between room temperature and 1800 K under ambient pressure. Z Metallkd. 2004;95(6):433–46.
38. Johnston WG, Gilman JJ. Dislocation velocities, dislocation densities, and plastic flow in lithium fluoride crystals. J Appl Phys. 1959;30(2):129–44.
39. De Souza RA. Oxygen diffusion in $SrTiO_3$ and related perovskite oxides. Adv Funct Mater. 2015;25(40):6326–42.
40. Meyer R, Waser R, Helmbold J, Borchardt G. Observation of vacancy defect migration in the cation sublattice of complex oxides by ^{18}O tracer experiments. Phys Rev Lett. 2003;90(10):105901.
41. Moon W-J, Ito T, Uchimura S, Saka H. Toughening of ceramics by dislocation sub-boundaries. Mater Sci Eng A. 2004;387–389:837–9.
42. Moon W-J, Saka H. Toughening of a brittle material by means of dislocation subboundaries. Philos Mag Lett. 2000;80(7):461–6.
43. Appel F, Messerschmidt U, Kuna M. Crack propagation in MgO during in-situ deformation in the high-voltage electron microscope. Phys Status Solidi A. 1979;55:529.
44. Rice JR, Thomson R. Ductile versus brittle behaviour of crystals. Philos Mag. 1974;29(1):73–97.
45. Xu G, Argon AS, Ortiz M. Critical configurations for dislocation nucleation from crack tips. Philos Mag A. 1997;75(2):341–67.
46. Nakamura A, Yasufuku K, Furushima Y, Toyoura K, Lagerlöf K, Matsunaga K. Room-temperature plastic deformation of strontium titanate crystals grown from different chemical compositions. Crystals. 2017;7(11):351.
47. Jin L, Guo X, Jia CL. TEM study of ⟨110⟩-type 35.26 degrees dislocations specially induced by polishing of $SrTiO_3$ single crystals. Ultramicroscopy. 2013;134:77–85.

How to cite this article: Salem MN, Ding K, Rödel J, Fang X. Thermally enhanced dislocation density improves both hardness and fracture toughness in single-crystal $SrTiO_3$. J Am Ceram Soc. 2023;106:1344–1355.
https://doi.org/10.1111/jace.18839